

Charge modification of the endothelial surface layer modulates the permeability barrier of isolated rat mesenteric small arteries

Paul M. A. van Haaren, Ed VanBavel, Hans Vink and Jos A. E. Spaan

Am J Physiol Heart Circ Physiol 289:2503-2507, 2005. First published Aug 12, 2005;

doi:10.1152/ajpheart.00587.2005

You might find this additional information useful...

This article cites 26 articles, 15 of which you can access free at:

<http://ajpheart.physiology.org/cgi/content/full/289/6/H2503#BIBL>

Updated information and services including high-resolution figures, can be found at:

<http://ajpheart.physiology.org/cgi/content/full/289/6/H2503>

Additional material and information about *AJP - Heart and Circulatory Physiology* can be found at:

<http://www.the-aps.org/publications/ajpheart>

This information is current as of May 8, 2007 .

Charge modification of the endothelial surface layer modulates the permeability barrier of isolated rat mesenteric small arteries

Paul M. A. van Haaren, Ed VanBavel, Hans Vink, and Jos A. E. Spaan

Department of Medical Physics, Cardiovascular Research Institute Amsterdam,
Academic Medical Center, University of Amsterdam, Amsterdam, The Netherlands

Submitted 2 June 2005; accepted in final form 25 July 2005

Van Haaren, Paul M. A., Ed VanBavel, Hans Vink, and Jos A. E. Spaan. Charge modification of the endothelial surface layer modulates the permeability barrier of isolated rat mesenteric small arteries. *Am J Physiol Heart Circ Physiol* 289: H2503–H2507, 2005. First published August 12, 2005; doi:10.1152/ajpheart.00587.2005.—We hypothesized that modulation of the effective charge density of the endothelial surface layer (ESL) results in altered arterial barrier properties to transport of anionic solutes. Rat mesenteric small arteries (diameter $\sim 190 \mu\text{m}$) were isolated, cannulated, perfused, and superfused with MOPS-buffered physiological salt solutions. MOPS-solutions were of normal ionic strength (162 mM, MOPS), low ionic strength (81 mM, LO-MOPS), or high ionic strength (323 mM, HI-MOPS), to modulate ESL charge density (normal, high, or low ESL charge, respectively). Osmolarity of MOPS, LO-MOPS, and HI-MOPS was kept constant at 297 mosmol/l, using additional glucose when necessary. Perfusate solutions were supplemented with 1% BSA. Arteries were cannulated with a double-barreled theta-pipet on the inlet side and a regular pipet on the outlet side. After infusion of FITC-labeled dextran of 50 kDa (FITC- $\Delta 50$) and the endothelial membrane dye 1,1'-dioctadecyl-3,3,3',3'-tetramethylindocarbocyanine perchlorate, the dynamics of arterial dye filling were determined with confocal microscopy. ESL thickness, as determined from the initial exclusion zone for FITC- $\Delta 50$ on the luminal endothelial surface, was $6.3 \pm 1.4 \mu\text{m}$ for LO-MOPS, $2.7 \pm 1.0 \mu\text{m}$ for MOPS, and $1.1 \pm 1.3 \mu\text{m}$ for HI-MOPS. At low ionic strength, FITC- $\Delta 50$ permeated into the ESL with a total ESL permeation time (τ_{ESL}) of 26 min, and at normal ionic strength with a τ_{ESL} of 20 min. No apparent exclusion of FITC- $\Delta 50$ from the ESL could be observed at high ionic strength. In conclusion, we demonstrate that the modulation of solvent ionic strength influences the thickness and barrier properties of the ESL.

vascular permeability; isolated artery; ionic strength; glycocalyx

THE LUMINAL SURFACE of vascular endothelium is coated with highly negatively charged proteoglycans and glycosaminoglycans, forming an endothelial surface layer (ESL) that contributes to the permselective barrier properties of the vascular wall (1, 10, 17, 24, 26). Well-known factors determining solute transport are size, conformation, and charge of solute molecules (1, 2, 8, 15, 16). This was demonstrated by Vink and Duling (26) in cremaster muscle capillaries by measuring the rate of uptake of fluorescently labeled dextrans in the ESL. In small cannulated arteries of $\sim 150 \mu\text{m}$, we found earlier that the ESL can be 2–3 μm thick (24). This was concluded from confinement of large anionic FITC-dextran molecules (FITC- $\Delta 148$; 148 kDa) to a core volume inside these arteries. FITC- $\Delta 50$ (50 kDa) was able to slowly permeate into the ESL, and the even smaller FITC- $\Delta 4$ (4 kDa) crossed the ESL relatively easily and accumulated in the arterial wall. An even larger ESL

thickness (7 μm) was predicted from studies (13) on coronary arteriolar permeability using an enzyme degradation technique.

Recently, Damiano and Stace (6, 22) developed an electrochemical model to predict ESL transport of charged molecules. This model predicts partial exclusion of anionic tracers from the ESL and attenuated transport of these tracers into the ESL over time, in agreement with the above mentioned arterial measurements (24). Because both the exclusion factor and tracer accumulation rate were predicted to depend on the volume density of fixed charges within the ESL and on the valence of solute tracers, it was hypothesized that a modulation of the ESL charge density by varying solvent ionic composition should influence the ESL barrier properties.

The present study was designed to demonstrate the effect of solvent ionic composition on ESL dimension and solute transport kinetics, applying our earlier developed technique to measure these properties using confocal laser scanning microscopy (CLSM). Solute transport through the ESL is characterized by convection and diffusion. Convection is dependent on the luminal solute concentration and the reflection coefficient of the arterial wall to the solute. Diffusion is dependent on the transvascular concentration gradient and the permeability of the arterial wall barrier to solute transport. MOPS-buffered physiological salt solutions (PSS) were used with either normal ionic strength, low ionic strength (LO-MOPS), or with high ionic strength (HI-MOPS), while maintaining isosmolarity for all three solutions.

MATERIALS AND METHODS

Artery preparation. All experiments were performed according to institutional guidelines. Male Wistar rats ($n = 21$, 200–250 g) were euthanized by decapitation, and the mesentery was excised and immediately put into cold (4°C) MOPS-PSS (see *Solutions*). A small artery was dissected from the mesentery and transported to the pressure myograph. Average internal diameter at 60 mmHg and full dilation was $189 \pm 6 \mu\text{m}$; no significant differences in diameter existed between the various groups of arteries in this study. Each rat provided one vessel. Other vessels or organs from the same rat were used in other experiments.

Myograph. The isolated artery was cannulated at one end with a double-barreled theta-cannula (World Precision Instruments) and at the other end with a regular glass cannula. The artery was pressurized and perfused with either MOPS-BSA, LO-MOPS-BSA, or HI-MOPS-BSA (see *Solutions*) at input and output pressures of 65 and 55 mmHg, respectively, by means of two Fairchild pressure regulators. This pressure difference resulted in a flow through the arteries of $3.4 \pm 0.5 \mu\text{l}/\text{min}$, as measured by a μFlow liquid mass flowmeter

Address for reprint requests and other correspondence: J. A. E. Spaan, Dept. of Medical Physics, Academic Medical Ctr., Univ. of Amsterdam, PO Box 22700, 1100 DE Amsterdam, The Netherlands (e-mail: j.a.spaan@amc.uva.nl).

The costs of publication of this article were defrayed in part by the payment of page charges. The article must therefore be hereby marked “advertisement” in accordance with 18 U.S.C. Section 1734 solely to indicate this fact.

(Bronkhorst Hi-Tec Holland), resulting in an estimated wall shear stress of 1.0 ± 0.2 dyn/cm². The artery could be perfused with a solution containing fluorescent tracers via the second barrel of the θ -cannula. Fluorescent perfusate was also pressurized to 65 mmHg. The superfusate, 37°C MOPS-PSS, LO-MOPS-PSS, or HI-MOPS-PSS (see *Solutions*) of which Po₂ was maintained at ambient values, was continuously recirculated with a roller pump. The PCO₂ was not controlled because pH was buffered by MOPS. Under these conditions these arteries were without tone and maintained a constant diameter during the protocol. Viability of the vessels was tested by the administration of norepinephrine and ACh; all vessels reacted normally to these agents.

Solutions. The MOPS-PSS contained (in mM) 145 NaCl, 4.7 KCl, 1.17 MgSO₄, 1.2 NaH₂PO₄, 2 CaCl₂, 3 MOPS, 5 glucose, and 2 pyruvate.

LO-MOPS-PSS was based on MOPS-PSS, with NaCl reduced to 64.2 mM to reduce ionic strength, and glucose increased to 153.8 mM to maintain isosmolarity. HI-MOPS-PSS was based on MOPS-PSS, with NaCl (38.2 mM) partially replaced by Na₂SO₄ (89.5 mM) to increase ionic strength while maintaining isosmolarity.

Ionic strength of MOPS-PSS was 162 mM, of LO-MOPS-PSS 81 mM, and of HI-MOPS-PSS 323 mM, according to its definition: ionic strength $\equiv \frac{1}{2} \sum c_i \cdot z_i^2$, where c_i is the concentration of ion i , and z_i is its valence. Osmolarity (Ω) for all three solutions was 297 mosmol/l, according to its definition $\Omega \equiv \sum \phi_i \cdot j_i \cdot c_i$, where ϕ_i is the osmotic coefficient of solute i , j_i is its number of particles formed on dissociation, and c_i is its concentration. Perfusate MOPS-PSS, LO-MOPS-PSS, and HI-MOPS-PSS were supplemented with 10 mg/ml BSA (99% pure), freshly applied before use in the experiments. All chemicals were purchased from Sigma. All solutions were adjusted to pH 7.35.

Fluorescent probes. FITC-labeled dextran of 50.7 kDa (FITC- Δ 50) was purchased from Sigma, and the lipophilic membrane tracer 1,1'-dioctadecyl-3,3',3'-tetramethylindocarbocyanine perchlorate (DiI) from Molecular Probes. FITC- Δ 50 was applied in a concentration of 45.0 mg FITC- Δ 50/l (9×10^{-7} M), resulting in a concentration of 1.0×10^{-6} M FITC. Labeling ratio for FITC- Δ 50 was 0.004 FITC/glucose molecule, according to the distributor. Therefore, the net anionic charge on FITC- Δ 50 is ~ 1.1 /dextran. FITC- Δ 50 was not filtered before use; thus there might be some free FITC present in the solutions. There might also be some polydispersion in the size of the dextran molecules. The possible contribution of free FITC and polydispersion will, however, be similar for all experiments in all groups of arteries. DiI was applied in a concentration of 1.0×10^{-5} M. Once incorporated in the endothelial membrane, DiI will stay there for the remainder of the experiment. DiI is able to spread along the membrane of an endothelial cell, but it cannot migrate from one cell to another (9, 11, 12).

Confocal microscopy. Images were recorded with a Leica DM IRBE microscope equipped with a Leica TCS SP2 confocal unit. Arteries were visualized from below through a cover glass that formed the bottom of the cannulation chamber. Excitation was obtained by an Ar ion laser using the 488 line. A $\times 20/0.70$ objective in combination with a zoom factor of 2 resulted in a pixel size of 366 nm \times 366 nm in the plane of focus. Green and red fluorescence were detected by using a prism and adjustable slits in front of two photomultipliers (PMTs). Wavelength of the detected light ranged from 500 to 530 nm (green) and from 625 to 750 nm (red), respectively. Crosstalk between both fluorescence channels was negligible. The detection pinhole was 20 μ m wide. Optical section thickness was about 13 μ m. In this protocol, most CLSM settings, including laser power, wavelength settings, and pinhole size, were identical for all experiments. However, high-voltage settings for the PMTs were not identical for all experiments in order to obtain an optimal dynamic range of the fluorescence images recorded during the different experiments. Consequently, fluorescence intensity was not directly comparable for all the recorded images. Therefore, we normalized FITC- Δ 50 fluores-

cence intensity to midluminal fluorescence before a comparison between different experiments. Images were recorded at midplane of the arteries every 3 s during the first 1.5 min of dye perfusion. During the remainder of the dye perfusion period (2–30 min), images were recorded every minute. Arteries were not illuminated between measurements to prevent phototoxic damage (27).

Image analysis. Profiles in radial direction were made of all fluorescence images, recorded at midplane, with the image analysis software ImageJ (National Institutes of Health). Measurement of the diameter of the arteries was based on the position of the endothelium, which was determined from the peak in the DiI fluorescence profiles, after subtraction of luminal DiI fluorescence (i.e., the profile after 1.5 min). FITC- Δ 50 fluorescence profiles, normalized to midluminal fluorescence intensity, were quantified in a region spanning from 10 μ m abuminally to 15 μ m luminally of the endothelium.

Optical LSFs. To quantify the effect of the optical transfer function of the microscope system on the measured dye distributions, we developed a correction procedure as previously described and verified (24). In short, the optical transfer function of the CLSM is characterized by a three-dimensional point-spread function (PSF) with a full-width half-maximum (FWHM) of ~ 3 μ m in the image plane, which increases at increasing distances from the plane of focus and with a FWHM in z -direction of ~ 13 μ m, i.e., the optical section thickness. The PSF results in a one-dimensional line-spread function (LSF), which we could estimate experimentally by direct observation of the DiI labeling of the endothelial membranes. Because the endothelium is only ~ 0.2 μ m in thickness, this can be considered as a line; thus the average DiI fluorescence profile can be used as a LSF. This LSF has a FWHM of ~ 5 μ m and is slightly asymmetric with respect to the endothelial position, because it takes the curvature of the endothelium along the arterial wall circumference into account. However, this does not impose any additional problem, because this asymmetry also reflects the curvature of the FITC- Δ 50 core inside the vessels. Convolution of this LSF with square-shaped FITC- Δ 50 arterial concentration profiles results in predicted FITC- Δ 50 fluorescence profiles, which were fitted to the measured fluorescence profiles after 2–30 min of FITC- Δ 50 perfusion to provide an estimate of the position of the FITC- Δ 50 front near the arterial wall. The square-shaped concentration profiles are characterized by a shift X_s from the endothelial position that represents the exclusion of FITC- Δ 50 from the ESL. Although the concentration profiles can be considered discontinuous, the fluorescence profiles will always be continuous due to the convolution with the continuous LSF. The rather wide LSF has the consequence that FITC- Δ 50 fluorescence intensity increases over a rather large distance from the endothelium, ~ 15 μ m, even if the dye concentration would be perfectly constant at this distance from the wall. Nevertheless, this procedure allows us to localize the FITC- Δ 50 concentration distribution with respect to the endothelial position with an accuracy of < 0.2 μ m and to quantify FITC- Δ 50 transport kinetics (24). These kinetics are expressed in terms of the total ESL permeation time (τ_{ESL}), the time needed for FITC- Δ 50 to pass the ESL and to reach the endothelium, i.e., the time needed for X_s to become ~ 0 μ m.

Statistics. Data are means \pm SE. The 95% confidence intervals were used to determine whether parameters were significantly different from 0 μ m. Parameters describing fluorescence profiles for the different solutions were compared using ANOVA and Bonferroni post hoc tests. The dilation in response to ACh for the different groups of arteries were also compared using ANOVA and Bonferroni post hoc tests. Paired t -tests were used for the comparison of parameters at 2 min versus 30 min. A value of $P < 0.05$ was considered significant.

RESULTS

After being cannulated, arteries were equilibrated at 37°C for at least 30 min. Endothelial viability was tested by an administration of 10^{-6} M ACh to the superfusate of arteries,

precontracted with 10^{-6} M norepinephrine (Nor). Ionic strength did not affect dilation in response to ACh [LO-MOPS, $58.9 \pm 9.1\%$; MOPS, $68.5 \pm 8.9\%$; and HI-MOPS, $53.8 \pm 11.2\%$; $P =$ not significant (NS)]. After these viability tests, Nor and ACh were washed out, and further measurements were obtained at full dilation.

To determine the spatial distribution of FITC- $\Delta 50$ over time, we measured fluorescence profiles from the recorded images during 30 min of dye perfusion for seven arteries in each group (LO-MOPS, MOPS, and HI-MOPS). Figure 1 provides the average fluorescence profiles in a region extending between 15 μm at the luminal side and 10 μm at the abluminal side of the endothelium, of cannulated arteries perfused and superfused with LO-MOPS (Fig. 1A), normal MOPS (Fig. 1B), or HI-MOPS (Fig. 1C). The position of the endothelium as determined from peak DiI fluorescence is taken as position 0 μm and is depicted with the vertical dotted lines. Figure 1 demonstrates that the development of the fluorescence profiles is slowest for LO-MOPS, faster for MOPS, and very fast for HI-MOPS, whereas after 30 min of dye perfusion, approximately identical fluorescence distributions are accomplished for the different groups of arteries. There were no significant differences in the fluorescence profiles after 30 min of dye perfusion for any of the three solutions.

Figure 2 shows the time dependence of X_s for LO-MOPS, MOPS, and HI-MOPS, representing the time-dependent permeation of FITC- $\Delta 50$ into the ESL for the different ionic strength conditions. The initial distance of FITC- $\Delta 50$ from the endothelial position, i.e., the value of X_s after 2 min of dye perfusion, represents the dimension of the ESL for the different ionic strength conditions. Initial X_s for LO-MOPS (6.3 ± 1.4 μm ; $P < 0.05$ vs. 0 μm) was higher than for MOPS (2.7 ± 1.0 μm ; $P < 0.05$ vs. 0 μm) and significantly higher than for HI-MOPS (1.1 ± 1.3 μm ; $P =$ NS vs. 0 μm).

For LO-MOPS, X_s decreased significantly during 30 min of dye perfusion from 6.3 ± 1.4 μm after 2 min to -0.2 ± 0.8 μm ($P =$ NS vs. 0 μm) after 30 min, with a total τ_{ESL} of ~ 26 min. For MOPS, X_s decreased significantly from 2.7 ± 1.0 μm ($P < 0.05$ vs. 0 μm) after 2 min to -0.7 ± 0.7 μm ($P =$ NS vs. 0 μm) after 30 min, with a τ_{ESL} of ~ 20 min. For HI-MOPS, no significant change in X_s occurred (from 1.1 ± 1.3 μm after 2 min to 1.0 ± 0.5 μm after 30 min), indicating no detectable exclusion of FITC- $\Delta 50$ from the ESL. There were no significant differences in X_s after 30 min among the three groups of arteries.

DISCUSSION

We demonstrate that modulation of solvent ionic strength affects the dimension of the ESL and its kinetics for FITC- $\Delta 50$ transport. Reduction of ionic strength increased ESL thickness and τ_{ESL} for FITC- $\Delta 50$, whereas an increase in ionic strength minimized ESL dimension and its barrier properties.

Criticism of method. To visualize arteries of 150–200 μm , we needed a long working distance objective with relatively low numerical aperture. This results in blurring of the images, which complicates the localization of fluorescent tracers even when using a confocal microscope. To circumvent this complication, we previously developed and verified a correction procedure to estimate the concentration distribution of the tracers inside the cannulated arteries (24). By obtaining X_s , the

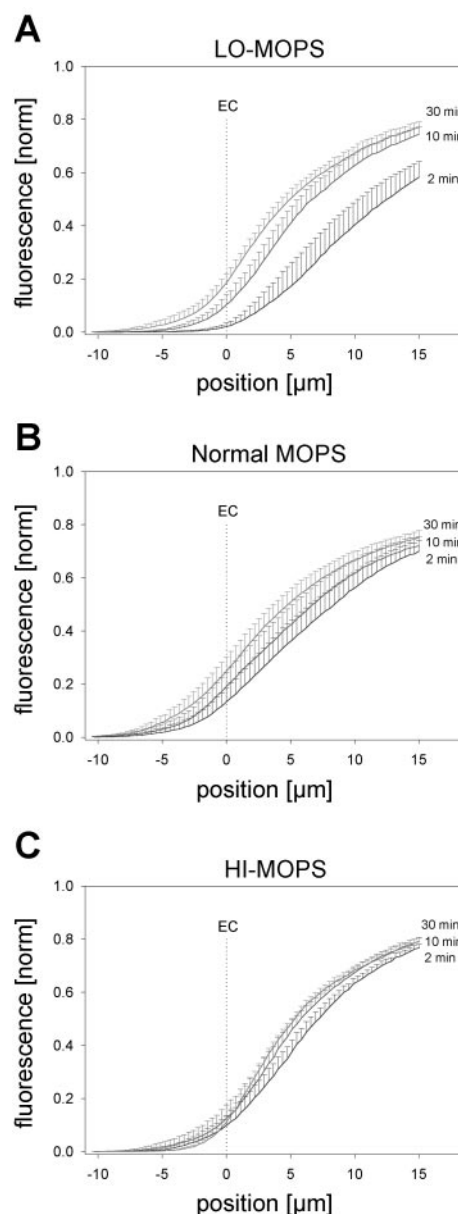


Fig. 1. Kinetics of average normalized FITC-labeled dextran of 50 kDa (FITC- $\Delta 50$) fluorescence in a region from 10 μm abluminally to 15 μm luminally of endothelium for arteries perfused and superfused with low ionic strength MOPS (LO-MOPS, A), normal MOPS (B), or high ionic strength MOPS (HI-MOPS, C). Fluorescence was normalized to midluminal fluorescence. Position of endothelium was determined from peak 1,1'-dioctadecyl-3,3,3',3'-tetramethylindocarbocyanine perchlorate (DiI) fluorescence and is depicted with dotted lines (endothelial cells, EC). Negative positions indicate abluminal from endothelium (arterial wall); positive positions indicate luminal from endothelium. Profiles values are means \pm SE; $n = 7$ experiments/group.

shift of the FITC- $\Delta 50$ concentration profile from the endothelial position, from 2 to 30 min of dye perfusion, we were able to study the kinetics of FITC- $\Delta 50$ transport through the ESL and the dependence of these kinetics on solvent ionic strength. This led us to substantiate that the ESL dimension, as determined from the luminal exclusion zone to FITC- $\Delta 50$ after 2 min of dye perfusion, as well as transport kinetics of FITC- $\Delta 50$ into the ESL are dependent on ionic strength. We did not obtain X_s for dye perfusion times < 2 min, because this would

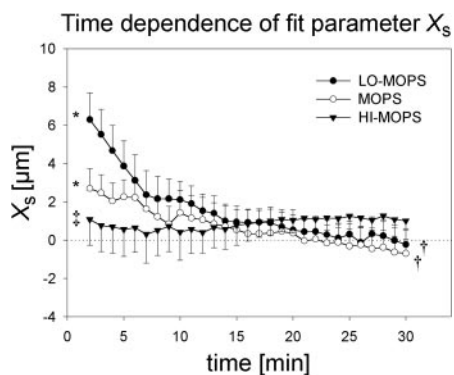


Fig. 2. Time dependence of fit parameter X_s from fits of FITC- $\Delta 50$ fluorescence profiles of LO-MOPS, MOPS, and HI-MOPS experiments, quantifying kinetics of FITC- $\Delta 50$ penetration into the endothelial surface layer (ESL). Value of X_s after 2 min of FITC- $\Delta 50$ perfusion, i.e., initial exclusion zone to FITC- $\Delta 50$, was used as measure for ESL thickness. Values are means \pm SE; $n = 7$ experiments/group. *Significantly different from 0 μm ; $\dagger P < 0.05$, 30 min vs. 2 min; $\ddagger P < 0.05$ vs. LO-MOPS.

be complicated due to inflow effects of FITC- $\Delta 50$ into the artery.

Significant cellular uptake or binding by the endothelium of FITC- $\Delta 50$ would have resulted in very different radial concentration profiles of FITC- $\Delta 50$ than the used square-shaped concentration profiles and would therefore have resulted in dissimilar fluorescence profiles than the observed fluorescence profiles. The present fluorescence profiles after 30 min of dye perfusion were still accurately described by square-shaped FITC- $\Delta 50$ concentration profiles convolved with the optical LSF for all groups of arteries. Furthermore, it has been previously demonstrated that FITC-labeled dextrans do not bind to the endothelium when albumin is present in the perfusate solution (7).

We concluded that the alterations in ionic strength did not influence the normal vascular wall integrity and function because ACh-derived dilation of the arteries was not affected by ionic strength. We did not confirm the calculated ionic strength or osmolarity for the different solutions by measurements, using, for example, freezing-point osmometers.

For practical reasons, we did not study whether the changes induced by ionic strength modulations could be reversed. Changing to solutions with a different ionic strength requires changing the superfusate as well as the perfusate of the arteries. The latter would require two additional lumina of the inflow cannula of the arteries, one for the second perfusate with different ionic strength and one for the second perfusate with fluorescent tracers. Therefore, we used only one solution (either LO-MOPS, MOPS, or HI-MOPS) per artery and compared the observed differences in FITC- $\Delta 50$ fluorescence profiles for seven arteries in each group.

In our experiments young male animals were used. It may be possible that the ESL properties with respect to ionic strength might change with sex or age of the animals or might even be different for different species. This was, however, beyond the scope of the present study.

Interpretation of results. Although a diminished transport of anionic solutes (2, 8, 15, 16) is in agreement with the presence of fixed negative charges on the luminal endothelial surface, the exact dimension of the endothelial structures carrying these negative charges has not yet been determined satisfactorily.

Imaging of the fixed negative charges after staining with cationic probes (1, 3, 14, 18, 19, 23) shows that the charges are mainly located in membrane-bound structures (glycocalyx) of the ESL, such as glycoproteins and proteoglycans, but these techniques usually fail to obtain insight into the true in vivo dimensions of the charge-carrying structures.

ESL volume is determined by a dynamic equilibrium of water movement into the ESL due to interactions among the charge-carrying structures of the glycocalyx, free plasma ions, and other charged molecules present in the perfusate and the hydrostatic pressure of the perfusate (6). On modification of one of these factors, the ESL will adapt its structural organization to a new dynamic equilibrium. Therefore, modulation of perfusate and superfusate ionic strength is likely to result in dimensional changes of the ESL as well as changes in ESL charge distribution, both affecting ESL permeability properties. In the present study, the dimension of the exclusion zone increased by a factor ~ 2.3 as ionic strength was decreased twofold (LO-MOPS compared with normal MOPS), whereas ESL thickness decreased by a factor ~ 2.5 as ionic strength was doubled (HI-MOPS compared with normal MOPS). There might be a very small influence zone of the ESL outside the thickness of the layer itself. Nevertheless, the so-called Debye-Hückel length of this zone is generally in the order of nanometers (5), which is negligible compared with the thickness of the ESL. Furthermore, it is not likely that the very low concentration of FITC- $\Delta 50$ (9×10^{-7} M) and its low anionic charge of $\sim 1.1/\text{dextran}$ has altered the ESL dimension or promotes aggregation of FITC- $\Delta 50$ molecules at the different ionic strengths.

Our findings support the predictions from the electrochemical model of Damiano and Stace (6, 22). Their model predicts the initial exclusion of anionic tracers from the ESL and the transport of these tracers into the ESL over time. Both issues are dependent on the charge density of the ESL and on the valence of the tracers. According to this model, cations present in blood partially counterbalance fixed negative charges in the ESL. These authors proposed to use variations in perfusate ionic composition to modulate ESL charge density and thereby influence the ESL transport of anionic tracers. It was predicted that a twofold decrease in ionic strength would result in a twofold increase in ESL charge density and a twofold increase in the voltage differential over the luminal blood-ESL interface that forms the actual physical barrier to transport of anionic molecules (6, 22). Furthermore, an increase in ionic strength was predicted to decrease ESL charge density and to attenuate exclusion of anionic molecules from the ESL. In the present study, a twofold decrease in ionic strength increased the ESL permeation time for FITC- $\Delta 50$ by only 30%, but this may be due to the co-occurring increase in ESL dimension, which may partially attenuate the predicted increase in ESL charge density. A twofold increase in ionic strength resulted in a decreased ESL dimension and a loss of its barrier properties, which is probably due to a collapse of matrix components and a loss of structural organization.

Sörensson and coworkers (20, 21) have studied the influence of perfusate ionic strength on the charge selectivity of the glomerular capillary wall. These authors demonstrated that lowering ionic strength 4.5-fold reduced the fractional clearance of several anionic tracers ~ 1.5 -fold, which was attributed to a reduction in the radius of the small pores responsible for

the exchange and to a reduction in the charge density of the glomerular barrier. A 1.9-fold increase in ionic strength resulted in a slightly increased fractional clearance of anionic tracers. The present study suggests, however, that these clearance effects are due to volume and charge density alterations of the charged gel that covers endothelial cells. Furthermore, Granger and coworkers (8) demonstrated that neutralization of the negative fixed charges on the intestinal capillary wall by infusion of polycations induces an approximately sixfold increase in permeability to fluid and approximately a fourfold increase in protein clearance.

A single study on direct conformational changes in red blood cell glycocalyx due to variations in ionic strength has been reported by Wolf and Gingell (28). These authors demonstrated that the red blood cell glycocalyx swells roughly by a factor ~ 2.2 as ionic strength falls by a factor 4. The swelling effects at low ionic strength might explain the large exclusion zone to FITC- $\Delta 50$ when using LO-MOPS observed in the present study.

Implications of the study. Because vascular permeability is fundamentally important for normal solute transport as well as for early alterations in a variety of pathologies, including inflammation or the development of atherosclerosis, a proper understanding of the physical properties of the vascular wall barrier is required. The present study demonstrates that charge distribution within the ESL plays a key role in the transport of large molecules. This study was designed as a proof of principle, to demonstrate an effect of ionic strength modulations on ESL dimension and its kinetics for solute transport. Although changes in ionic strength as applied in the current study do not normally occur, effects on ESL dimension and charge density may also result from oxidative stress (4, 25–27), and the resulting alterations in transport properties may form a very early event in vascular pathologies.

REFERENCES

1. Adamson RH and Clough G. Plasma proteins modify the endothelial cell glycocalyx of frog mesenteric microvessels. *J Physiol* 445: 473–486, 1992.
2. Adamson RH, Huxley VH, and Curry FE. Single capillary permeability to proteins having similar size but different charge. *Am J Physiol Heart Circ Physiol* 254: H304–H312, 1988.
3. Baldwin AL, Wu NZ, and Stein DL. Endothelial surface charge of intestinal mucosal capillaries and its modulation by dextran. *Microvasc Res* 42: 160–178, 1991.
4. Constantinescu AA, Vink H, and Spaan JAE. Elevated capillary tube hematocrit reflects degradation of the glycocalyx by oxidized low density lipoproteins. *Am J Physiol Heart Circ Physiol* 280: H1051–H1057, 2001.
5. Curry FE. Mechanics and thermodynamics of transcapillary exchange. In: *Handbook of Physiology*. The Cardiovascular System. *Microcirculation*. Bethesda, MD: Am Physiol Soc, 1984, sect. 2, vol. IV, pt. 1, chapt. 8, p. 309–374.
6. Damiano ER and Stace TM. A mechano-electrochemical model of radial deformation of the capillary glycocalyx. *Biophys J* 82: 1153–1175, 2002.
7. Gonzalez-Castillo C, Rubio R, and Zenteno-Savin T. Coronary flow-induced inotropism is modulated by binding of dextrans to the endothelial luminal surface. *Am J Physiol Heart Circ Physiol* 284: H1348–H1357, 2003.
8. Granger DN, Kvietys PR, Perry MA, and Taylor AE. Charge selectivity of rat intestinal capillaries. Influence of polycations. *Gastroenterology* 91: 1443–1446, 1986.
9. Haugland RP. *Handbook of Fluorescent Probes and Research Chemicals*. Eugene, OR: Molecular Probes, 1996.
10. Henry CBS and Duling BR. Permeation of the luminal capillary glycocalyx is determined by hyaluronan. *Am J Physiol Heart Circ Physiol* 277: H508–H514, 1999.
11. Hiscox S and Jiang WG. Quantification of tumour cell-endothelial cell attachment by 1,1'-dioctadecyl-3,3,3',3'-tetramethylindocarbocyanine (DiI). *Cancer Lett* 112: 209–217, 1997.
12. Honig MG and Hume RI. Fluorescent carbocyanine dyes allow living neurons of identified origin to be studied in long-term cultures. *J Cell Biol* 103: 171–187, 1986.
13. Huxley VH and Williams DA. Role of a glycocalyx on coronary arteriole permeability to proteins: evidence from enzyme treatments. *Am J Physiol Heart Circ Physiol* 278: H1177–H1185, 2000.
14. Palade GF, Simionescu M, and Simionescu N. Differentiated microdomains on the luminal surface of the capillary endothelium. *Biorheology* 18: 563–568, 1981.
15. Parker JC, Miniati M, Pitt R, and Taylor AE. Interstitial distribution of charged macromolecules in the dog lung: a kinetic model. *Ann Biomed Eng* 15: 157–172, 1987.
16. Perry MA, Benoit JN, Kvietys PR, and Granger DN. Restricted transport of cationic macromolecules across intestinal capillaries. *Am J Physiol Gastrointest Liver Physiol* 245: G568–G572, 1983.
17. Pries AR, Secomb TW, and Gaetgens P. The endothelial surface layer. *Pflug Arch* 440: 653–666, 2000.
18. Simionescu M, Simionescu N, Silbert JE, and Palade GE. Differentiated microdomains on the luminal surface of the capillary endothelium. II. Partial characterization of their anionic sites. *J Cell Biol* 90: 614–621, 1981.
19. Simionescu N, Simionescu M, and Palade GE. Differentiated microdomains on the luminal surface of the capillary endothelium. I. Preferential distribution of anionic sites. *J Cell Biol* 90: 605–613, 1981.
20. Sorensson J, Ohlson M, and Haraldsson B. A quantitative analysis of the glomerular charge barrier in the rat. *Am J Physiol Renal Physiol* 280: F646–F656, 2001.
21. Sorensson J, Ohlson M, Lindstrom K, and Haraldsson B. Glomerular charge selectivity for horseradish peroxidase and albumin at low and normal ionic strengths. *Acta Physiol Scand* 163: 83–91, 1998.
22. Stace TM and Damiano ER. An electrochemical model of the transport of charged molecules through the capillary glycocalyx. *Biophys J* 80: 1670–1690, 2001.
23. Ueda H, Takehana K, Eerdunchaolu Iwasa K, Fujimori O, and Shimada S. Electron microscopic cytochemical studies of anionic sites in the rat spleen. *J Vet Med Sci* 63: 287–291, 2001.
24. Van Haaren PM, VanBavel E, Vink H, and Spaan JA. Localization of the permeability barrier to solutes in isolated arteries by confocal microscopy. *Am J Physiol Heart Circ Physiol* 285: H2848–H2856, 2003.
25. Vink H, Constantinescu AA, and Spaan JAE. Oxidized lipoproteins degrade the endothelial surface layer. Implications for platelet-endothelial cell adhesion. *Circulation* 101: 1500–1502, 2000.
26. Vink H and Duling BR. Capillary endothelial surface layer selectively reduces plasma solute distribution volume. *Am J Physiol Heart Circ Physiol* 278: H285–H289, 2000.
27. Vink H and Duling BR. Identification of distinct luminal domains for macromolecules, erythrocytes, and leukocytes within mammalian capillaries. *Circ Res* 79: 581–589, 1996.
28. Wolf H and Gingell D. Conformational response of the glycocalyx to ionic strength and interaction with modified glass surfaces: study of live red cells by interferometry. *J Cell Sci* 63: 101–112, 1983.